

Electrochemical Simulation of the Current and Potential Response in Sliding Tribocorrosion

N. Papageorgiou · S. Mischler

Received: 29 March 2012 / Accepted: 28 July 2012 / Published online: 17 August 2012
© Springer Science+Business Media, LLC 2012

Abstract Valuable insights into the wear-corrosion behavior of metals, as well as into the tribocorrosion field through the development of simulation models of tribocorrosion experiments, can contribute in rationalizing wear-accelerated experiments and their open circuit potential (OCP) behavior under rubbing. These results demonstrate that mathematical models of controlled tribo-electrochemical contacts can complement the physical experiment and add valuable understanding to the tribological behavior of metals, alloys, and generally to materials in an electrochemically active environment. The excellent agreement of experimental wear data and the experimental OCP curves with the OCP simulations with time establishes the concepts underlying the galvanic coupling model as a valid methodological approach toward a quantitative description and mechanistic understanding of the tribo-electrochemical experiment. Besides analyzing stellite tribocorrosion, application of the model to Al alloy data has helped us quantify the relative contributions of chemical and mechanical wear and reveal the underlying synergy. Ti metal tribocorrosion under variable load has revealed that the contact pressure P_{av} , can reach much lower values within the experimental time domain and finally be the cause of interruption of the initial wear mechanism.

Keywords Tribocorrosion · Tribo-electrochemistry · Modeling · Corrosive wear · Galvanic coupling · Stellite · Titanium · Aluminum alloys

1 Introduction

Interesting approaches have appeared in the recent literature concerning the fundamental interpretation and the modeling of the repassivation kinetics during tribocorrosion [1–3] and the potential evolution with time for, e.g., freshly guillotined Al [4, 5], but none—as far as the authors are aware—have treated or attempted theoretically to reproduce the complex behavior and the time evolution of the quasi steady-state depassivation–repassivation response of a tribocorrosion sliding experiment, where any perturbation in the potential occurs over the entire electrode surface and the response is a convolution of that from the passive metal surrounding the scratch and that from the relatively very thin scratch itself.

The electrochemical conditions established in tribocorrosion systems play a crucial role for wear and friction. The prevailing electrode potential was found to govern not only electrochemical reactions such as repassivation of abraded surfaces but also the mechanical response of metals to friction. This study was initiated with the aim to theoretically understand open circuit potential (OCP) variation during tribocorrosion of certain model systems including a biomedical version of stellite 21 in sulfuric acid under plastic loading against a hard ceramic counter piece; to interpret the effects observed when variable loads are applied on Ti grade 2 metal in NaCl solution; and to perform a fresh evaluation of experimental data by quantitatively analyzing the factors contributing to the differences reported in the tribocorrosion behavior of Al alloys prepared and

N. Papageorgiou (✉)
Tribology Laboratory, Department of Engineering Design
and Materials, Faculty of Engineering and Technology, NTNU,
N-7491, Trondheim, Norway
e-mail: nikolaos.papageorgiou@ntnu.no

S. Mischler
Tribology and Interfacial Chemistry Group, Ecole Polytechnique
Fédérale de Lausanne (EPFL), 1015, Lausanne, Switzerland

studied elsewhere [6]. However, one can consider the results of the above particular assessments as a demonstration of the successful application of a unifying set of principles in tribocorrosion. To this end, this study indeed attempts to validate the developed OCP tribocorrosion model through its applicability to experimental data derived from chemically diverse systems, both in terms of corrosion-tested metal/alloy as well as corrosive environment such as electrolyte chemistry and normal load, with the ultimate intention to be able to substantiate the more generalized application of the fundamental principles and general assumptions of such a model to a wider range of tribo-electrochemical systems and tribocorrosion conditions.

The scope/rationale of such an approach is to develop the necessary conditions for a predictive theoretical model for a tribo-electrochemical sliding experiment able to characterize the real electrochemical conditions established in the tribological contact (wear track), ultimately aiming to numerically determine or predict the chemical reaction of the metals as well as their mechanical response under tribocorrosion. The theoretical model should include the galvanic coupling between anode (rubbed) and cathode (unrubbed) areas during tribocorrosion and the simplifying assumption of a uniform current distribution over the wear track. The model results would then be compared to experimental results from metallic samples (e.g., CoCrMo alloy, Ti metal, Al alloys, etc.) to assess its validity and application limits.

Because of the complexity of the involved phenomena, tribocorrosion mechanisms are not well understood, and general predictive models still lack. For this reason, a considerable amount of research was devoted in the past to the understanding of stellite tribocorrosion. Main attention was set on biomedical applications [7–9], and only a few on nuclear industry applications concerning stellite 6 [7, 10].

As the environment inside the human body is corrosive, the assessment of biomaterials to corrosion and corrosive wear is strongly required to ensure their safety. Pure titanium and its alloys are known as biomaterials because of their high corrosion resistant properties, and are applied to the implantation to fix broken bones. Most tribocorrosion studies of their properties as biomaterials are conducted in the presence of NaCl or Hanks' solution [11–14].

Some authors report that tribocorrosion of Al alloys in NaCl based solutions is characterized by adhesive wear, abrasive wear and plastic deformation [15–17]. In the case of passive aluminum, one would expect a significant increase in corrosion rate due to the mechanical removal of the passive film and the exposure of bare metal to the solution. The preparation and tribological testing of age-hardened Al–10Si–4.5Cu–2Mg (wt%) cast alloys was

investigated elsewhere [6], but better insight into the wear and electrochemical response of aluminum alloys subject to tribocorrosion in aqueous solutions can be achieved through mathematical modeling.

The mechanical and electrochemical deterioration mechanisms of these three model materials were investigated under severe sliding for their wear and open circuit electrochemical responses. Although the wear and corrosion behaviors of the above systems have been investigated, the available information was focused on the wear behavior and not on the interpretation of the OCP curves, as the fundamental interdependencies between wear, rubbing time, and OCP response had not been demonstrated.

Hence, the novel aspect in the present research is the analysis of the electrochemical response of not only Al alloys under rubbing, but also Ti metal and CoCrMo alloy to discover their global or common features, i.e., the principles that govern OCP response and the association of their electrochemical behavior with wear rates and other independent physical and electrochemical characteristics of each system. The unifying approach attempted in this study mainly consists in the development of a galvanic coupling model to analyze and quantitatively predict the evolution of the OCP during tribocorrosion, under the basic premise and the assumption of an established galvanic coupling between the whole depassivated wear track and the surrounding area of the test sample.

This study appears to be the first quantitative galvanic coupling model (depassivated vs passive areas of test sample) predicting the potential evolution during tribocorrosion and should thus provide new valuable insights into the wear-corrosion behavior of passive materials, as well as pave the way for further theoretical interpretation in the field of tribocorrosion. In the model systems selected, the correlation of the mathematically simulated cathode potentials, E_c , with the measured experimental OCP evolution curves has been good enough to validate such an approach.

2 Model Conditions: Mathematical Formulation

In typical engineering situations, the electrode potential is not imposed through an external potentiostatic circuit and can thus vary with time depending on the variability of the experimental conditions. The electrode potential spontaneously establishing between metal and solution is thus called OCP. Rubbing may significantly shift the OCP values because a galvanic coupling establishes between the depassivated worn area and the surrounding passive surface. As the electrode potential drives the electrochemical reactions, its evolution in the course of rubbing is a critical factor affecting metal oxidation and overall degradation.

The variation of OCP during an experiment can be easily monitored using an appropriate reference electrode connected to the investigated metal through a voltmeter. However, so far, no theoretical models are available for its quantitative interpretation, and thus the useful information extractable from OCP measurements is at present rather limited despite the practical relevance for tribocorrosion of engineering systems. For this reason, a simple galvanic coupling model commonly used in corrosion [18] was adapted to the tribocorrosion situation to mechanistically interpret the evolution of OCP during rubbing.

2.1 Galvanic Cell Model for Tribocorrosion at Open Circuit Potential

The cathodic shift of potential usually observed during tribocorrosion of passive metals can be explained by the galvanic coupling established between the mechanically depassivated areas (anode) and the surrounding passive areas (cathode). The depassivated areas act as anode where metal oxidation is the dominating phenomenon of the electrochemical reaction. Anodic oxidation leads to metal dissolution and, if the time interval between two successive passes is high enough, then it leads to the regrowth of the passive film. In neutral solutions, the reduction of water and/or oxygen is the dominating cathodic reaction. A galvanic ionic current can flow from the anode through the solution to the cathode where electrons liberated at the anode by the metal oxidation and flowing through the metal are consumed by the reduction reaction. Note that reduction of water and oxygen occurs in principle also on the anodes: however, this contribution is neglected here because in the present experiments the worn area is much smaller than the electrode surface area. In a galvanic cell, the anodic current I_a is equal to the absolute cathodic current I_c (as convention, cathodic currents are negative while anodic are positive). Considering the cathodic i_c and anodic i_a current densities (current per unit area), one can write for the case of tribocorrosion experiments:

$$I_a = -I_c \Leftrightarrow i_a A_a = -i_c A_c \quad (1)$$

where A_a and A_c correspond to the surface areas of the anode and the cathode, respectively. Here it is assumed that the current density is homogenous over the cathodic and anodic sites. In reality, much localized variations in galvanic current can be expected because of the deformed state of the rubbed metal. Indeed, Krawiec et al. [19] observed, using SVET, heterogeneities in anodic current distribution within wear tracks formed on stainless steel.

The relation between cathode potential E_c and the current density i_c can be determined empirically by a Tafel extrapolation of the linear part of the cathodic branch of the polarization curve:

$$E_c = E_{corr} + a_c - b_c \log|i_c| \quad (2)$$

where a_c and b_c are constants and E_{corr} the corrosion potential of the passivated metal (i.e., the potential at which the current changes sign in the polarization curves). Combining Eqs. (1) and (2) yields

$$\begin{aligned} E_c &= E_{corr} + a_c - b_c \log(i_a A_a / A_c) \\ &= E_{corr} + a_c - b_c \log i_a - b_c \log(A_a / A_c) \end{aligned} \quad (3)$$

According to Eq. (3), the cathode potential in the galvanic coupling depends mainly on two factors: the anodic current and the anode-to-cathode area ratio. The anodic current is, owing to the cyclic depassivation/repassivation process, established in the rubbed area. Between two strokes, the passive film grows in the depassivated areas up to a certain thickness depending on the stroke frequency, electrode potential, and passivation kinetics. The film's regrowth requires a certain anodic charge density (passivation charge density q_p in C/m²). Accordingly, the current density i_a is given by Eq. (4) where f is the stroke frequency (Hz):

$$i_a = q_p f \quad (4)$$

Equation (4) implies that the current i_a does not change in the course of an experiment at constant potential. In the case of OCP tribocorrosion tests, q_p is expected to change to some extent during the initial potential drop but to remain nearly constant once a steady-state potential is reached during tribocorrosion. The anodic current density i_a corresponds to the passivation charge density passed at each stroke to repassivate the wear track, which normally obtains a steady value during the tribocorrosion of passive metals. In this model, it would be generally more correct to assume an i_a representing an average value established during the steady-state tribocorrosion and after an initial stabilization period of the tribocorrosion experiment mentioned earlier. With respect to the overall correlation of wear and the repassivation current at steady-state, the considered practical order of magnitude for i_a as described by Eq. (4), for a given tribological system during the rubbing phase in wear-accelerated corrosion experiments, has been exemplified by Landolt et al. [20] in an analysis on the dependence of the anodic current on the repassivation charge and the generation rate of depassivated surface, which leads to a general expression for the current density i_a that is independent of time or cycle number.

In tribocorrosion, either of two limiting galvanic coupling situations can theoretically arise: (1) galvanic coupling between the completely depassivated wear track and the area surrounding it, or (2) short-range galvanic coupling between depassivated and still passive areas within the wear track and on the area immediately surrounding the wear track (this latter area is expected to be negligible in case of large wear

tracks and therefore it is not considered here). Films that are mechanically weak and easy to remove should promote the former situation, while adherent, thick, and resistant passive films lead to the latter. High loads should also favor the complete depassivation of the wear track. In real cases, both limiting situations are likely combined, and galvanic coupling may occur between depassivated area and passive areas within and outside the wear track. The evolution of the A_a/A_c ratio during rubbing depends on the coupling situation. In the case of galvanic coupling within the wear track, this ratio depends on the percentage of depassivated area inside the wear scar. This percentage is not expected to change during an experiment and does not depend significantly on normal force as long as the contact pressure remains high enough to provoke large plastic deformation and depassivation. In the case of the galvanic coupling between the whole wear track and surrounding area, the A_a/A_c ratio increases significantly with the progress of wear and the corresponding enlargement of the wear track. Further, this ratio is expected to increase proportionally to the applied load as wear becomes more severe. This simple model allows one to relate the evolution of the electrode potential during a tribocorrosion test with the extent of wear and thus to mechanical and material properties. Also the influence of the cathodic current or cathode kinetics can also be assessed.

2.2 Quantitative Prediction of Potential Drop in Case of Galvanic Coupling Between Wear Track and Surrounding Area

For the situation illustrated above, Eq. (3) can be used to quantitatively evaluate the evolution of the OCP during rubbing by assuming that the wear track area A_{wt} corresponds to the anodic area A_a , while the rest of the electrode surface constitutes the cathode with area A_{owt} (area outside the wear track). As a consequence of progressing wear, A_{wt} increases with rubbing time.

The wear track area A_{wt} corresponds to the wear track length multiplied by the arc length of the circular segment defined by the wear track:

$$A_{wt} = LR\theta \quad (5)$$

The wear track area A_{wt} is related to the instantaneous wear track volume. The wear track volume V can be approximately calculated by multiplying the stroke length L by the area of the circular segment (A_{cs}) defined by the alumina ball of radius R impinging upon the metal according to Eq. (6):

$$V = LA_{cs} = 0.5LR^2(\theta - \sin\theta) \quad (6)$$

where θ (rad) is the central angle defining the circular segment. For angles lower than 0.6 (i.e., wear scar width

lower than 1.75 mm), Eq. (6) can be empirically simplified with less than 1 % error by Eq. (7):

$$V = 0.08333LR^2\theta^3 \quad (7)$$

In addition, according to Archard's wear law, a linear relationship between the wear volume (V) and rubbing time (t) can be assumed:

$$V(t) = C_w t \quad (8)$$

where C_w is the wear constant that can be calculated by dividing the wear track volume measured at the end of the test by the rubbing duration. Extracting θ from Eq. (7) and considering Eq. (8) to define V , Eq. (5) can be rewritten as

$$A_{wt} = (L^2 R C_w t / 0.0833)^{0.333} \quad (9)$$

Therefore, E_c can be defined as

$$E_c = E_{corr} + a_c - b_c \log i_a - b_c \log [(L^2 R C_w t / 0.0833)^{0.333} / A_{owt}] \quad (10)$$

where a_c and b_c are the Tafel parameters determined by interpolation of the cathodic branch of the polarization curve, values of which need to be determined experimentally. In cases of non-ideal Tafel behavior of the cathodic polarization, the analytic solution of Eq. (10) cannot be directly applied, and the E_c determination relies on the interpolation of calculated current values on the polarization curve. It is noted that the polarization commenced from the equilibrium state at the corrosion potential and the scan directed toward cathodic potentials to better reflect the conditions that the cathode area would experience during the rubbing phase of the tribocorrosion experiment. This procedure best minimizes the possible total or partial dissolution/alteration of the passive layer of the cathode. In principle, the surface area outside the wear track, A_{owt} , is a function of time, but owing to the small size of the wear track compared with the overall electrode, we can reasonably assume that in the present case A_{owt} is constant with time and corresponds approximately to the electrode area.

One may want to question the notion whether the experimentally recorded OCP and the mathematically generated E_c values are physically and/or conceptually the same quantity. The fact that they represent the same physical quantity becomes clearer when the experimentally measured OCP is understood as the actual potential difference between the reference electrode and the cathode area of the experimental sample—and not the wear track (anode). The comparison of mathematically simulated E_c curves and measured experimental OCP values, is valid, as the OC potential under rubbing is indeed the cathodic potential E_c , resulting from the cathodic process driving the anodic reaction [4]. Admittedly, this fact is not always easy to discern under the present experimental setup, and one

must resort to the predominance of the cathode geometrical surface, the form of the equipotential surfaces, and their conformal current distribution emanating from the cathode area and reaching the reference electrode tip, to dispel doubts surrounding the nature of the physically measured OC potential being monitored during the tribological rubbing experiment.

Moreover, the anode potential values E_c calculated here for the quasi steady-state sliding experiment are the equivalent of the potential analyzed by Burstein et al. (referred there as OCP [5]), in their guillotined Al experiments, as in our case the wear track is not isolated and its potential is here monitored as the response from the surrounding cathode. However, even when correlating these two, one should understand the sample bulk potential response as a quantity that results from the sequential mechanical depassivation and subsequent repassivation currents of infinitesimal bared or mechanically denuded specimen surfaces within the wear track at a given rate over the whole sliding cycle or period. Supporting evidence to the above is the good correlation between our model predicted potential values for Al alloys [6] and the OC potentials measured in the guillotined Al experiments reported in [5] within the appropriate time scale of ca. 0.1–1 s.

3 Experimental Details

All reported tribocorrosion experiments were performed on a reciprocating motion tribometer equipped with an electrochemical cell used to carry out tests at open circuit conditions. Although the applied load varied, all experiments were conducted at a frequency of 1 Hz and with a stroke length of 5 and 4 mm for the Al alloys. The polycrystalline alumina balls (99.8 % Al_2O_3 supplied by SWIP AG Brugg) used as counter piece were 6 mm in diameter and exhibited, according to the manufacturer, the following values: R_a roughness of 0.020 μm , a Young's Modulus of 360 GPa, and a Poisson's ratio of 0.22. The tests were performed in 0.14 M, 0.05 M NaCl electrolyte or in 0.5 M H_2SO_4 solution, and the sample area exposed to the electrolyte was 3.8 cm^2 .

3.1 Tribometer

Reciprocating sliding tribocorrosion tests were carried out for all samples in this study with the sliding tribo-electrochemical apparatus, details of which are given in a separate publication [21]. This reciprocating pin-on-plate tribometer has a back-and-forth movement caused by a linear motor ALS that is driven by an Aerotech's Soloist device controlling the amplitude and the velocity of the displacement

and the dwell time at direction reversal during reciprocating motion. A PP electrochemical cell is fixed over the motor. The three-electrode system is composed of a reference electrode: a mercury sulfate electrode or Ag/AgCl ; a counter-electrode: a platinum wire in spires that is placed around the sample; and a working electrode, the sample. The electrodes are connected to a Bank Wenking LB 95L potentiostat. The alumina ball fixed to a three-component force sensor KISTLER 9251 is fixed on a vertically mounted shaft held by a linear ball bearing. This quartz force sensor permits to measure the orthogonal components of a dynamic or quasi static force emitting an electrostatic signal proportional to the acting force. The load is applied on the other end of the shaft by means of appropriate dead weights. The vertical position of the shaft is maintained by a spring (constant 2.4 N/mm) placed around it, which compensates for the shaft's weight and thus allowing one to apply smaller forces. The table displacement is monitored for control purposes through a laser diode coupled with a position-sensitive device PSD (Hamamatsu). The electrochemical (current, potential), force (normal force, friction force), and displacement (x, z) values are continuously monitored at a sampling rate of 1 k sample/s and treated by an acquisition system based on a analog/digital board installed in a personal computer (PC) and controlled by a home-developed software based on Lab view.

3.2 Tribocorrosion of Stellite 21 in 0.5 M H_2SO_4

The CoCrMo alloy used was a high carbon alloy (HC-CoCrMo). Its chemical composition by element weight percent was Co Balance, Cr 26.0–30.0, Mo 5.0–7.0, C 0.20–0.25 Ni max 1.0.

The samples were disks of 24 mm diameter and 4 mm high.

Post-test characterization of the worn surfaces was carried out using optical microscopy and non-contact scanning laser profilometry. Calculation of the total wear volume V_w was done from graphical integration of the wear track's cross-section obtained by scanning laser profilometry.

Normal load applied was 11.7 N

3.3 Tribocorrosion of Ti Metal in 0.14 M NaCl

The pure Ti (99.6 %) samples were in the form of disks of 24-mm diameter and 4-mm thickness.

Normal loads applied were 7, 3, and 0.5 N

Control and measurements of the wear volume V_w were done from the wear track's profile obtained by means of the Mitutoyo SJ-301 profilometer-surface roughness tester (total volume loss was obtained by multiplying the average area of the cross-sectional profiles by the stroke length) and by means of confocal microscopy (IFM Alicona).

3.4 Tribocorrosion of Al Alloys in 0.05 M NaCl

The tribocorrosion of Al–10Si–4.5Cu–2Mg (wt%) alloys was investigated in 0.05 M NaCl solutions under severe sliding and controlled electrochemical conditions; the preparation as well as experimental details are reported elsewhere [6]. The applied normal load of 4 N was the same for all Al alloys. Here, the comparison of Al-NHT and very similar behaving Al-S2h and Al-S8h with respect to OCP versus time and total V_w is mainly emphasized.

All polarization curves were recorded at 0.5 mV/s in air and in their corresponding tribocorrosion electrolyte by scanning the potential from the sample corrosion potential in the cathodic direction after a minimum of 10-min rest at equilibrium.

Before polarization and tribocorrosion test, the samples were polished in water using SiC paper from 500 to 4000 mesh. Final polishing was performed using diamond particles of 1 μm (Struers lubricant). The obtained surfaces were ultrasonically cleaned in ethanol during 5 min and then rinsed in distilled water and dried with compressed air.

4 Simulation Model: Results and Discussion

4.1 Stellite 21 in 0.5 M H₂SO₄

The cathode's electrochemical kinetics, vital to the model E_c determination, were extracted from the experimental polarization curve (Fig. 1) produced under similar electrode–electrolyte conditions to the tribocorrosion tests. The wear volume data obtained from the measurement technique of graphical integration of the wear scar profile defines a straight line with rubbing time as seen in Fig. 2, indicating the experimental validity of Archard's law in

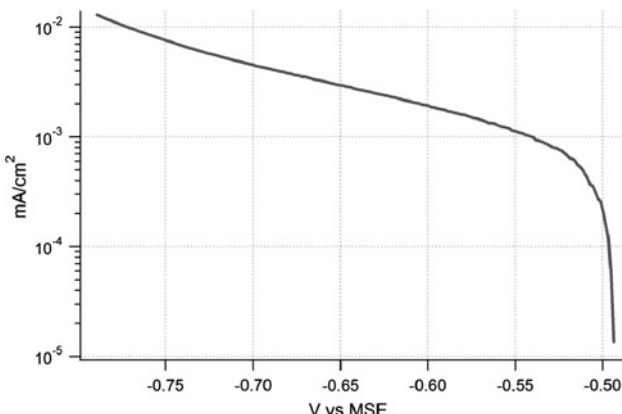


Fig. 1 The cathodic polarization curve for the stellite 21 sample in 0.5 M H₂SO₄ which was utilized in the tribo-electrochemical OCP model

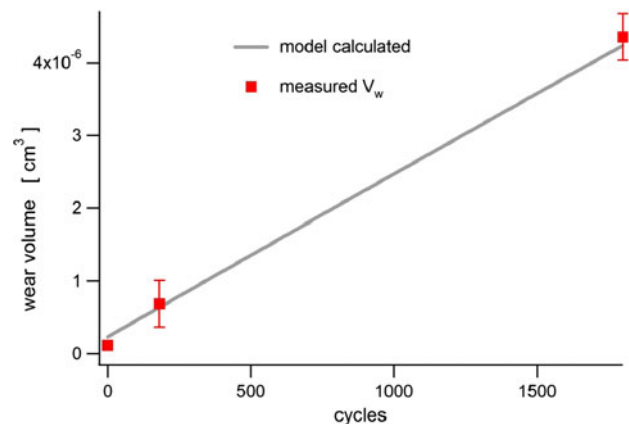


Fig. 2 The total wear volume experimental data plotted against the model's calculated volume loss as a function of time for the stellite 21 sample in 0.5 M H₂SO₄ system under tribocorrosion at 11.7 N normal load

this case. On the basis of best fitting the experimental wear volume data of the system under the conditions modeled, i.e., stellite 21, 0.5 M H₂SO₄ and load condition 11.7 N, the model parameter of $i_a = 1.19 \text{ mA/cm}^2$ was determined. It should be emphasized at this point that, owing to the apparent disparity in the recorded polarization curves, and as a consequence of the choice of experimental conditions (e.g., prior cathodic cleaning, equilibration time, and extent of anodic excursion before cathodic polarization or the general irreproducibility of surface preparation, catalytic state of the sample surface, etc.), the parameter i_a can vary within a range of tolerance, estimated at ca. $\pm 13\%$. The simulation of the tribo-electrochemical experiment for the above normal load and current density inside the wear track, i_a , gives a wear volume–time evolution curve which is linear, as it is derived from the theoretical validity of Archard's law, with the slope of this plot being the wear constant C_w . When fitted to the measured wear volume data, the model gives a calculated value $C_w = 2.45 \times 10^{-9} \text{ cm}^3/\text{s}$ for Archard's behavior:

$$V [\text{cm}^3] = C_w * t [\text{s}] \quad (11)$$

The model's calculated slope value C_w from the straight line of wear volume with time is in very good agreement with the experimental values, which are clearly well within the standard deviation (SD) of the wear volume measurement. The determination of the wear constant C_w [or knowledge of the value for the dimensionless wear coefficient K_w , see Eq. (12)] is obviously vital in any attempt to apply Archard's wear equation in a predictive fashion.

According to Hertz contact theory, the contact area diameter of the spherical pin on the planar sample, given also the mechanical properties of stellite 21, is theoretically 110 μm before the initiation of rubbing. It is noted here

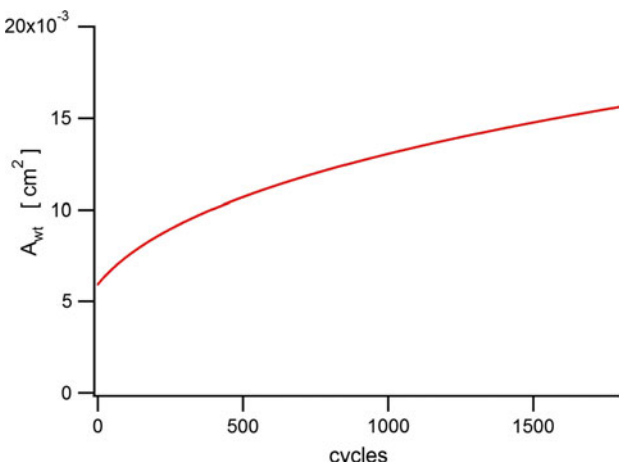


Fig. 3 The plot of wear track's surface area with time as calculated from model for the stellite 21 sample in 0.5 M H₂SO₄ under tribocorrosion at 11.7 N normal load and the experimental conditions mentioned

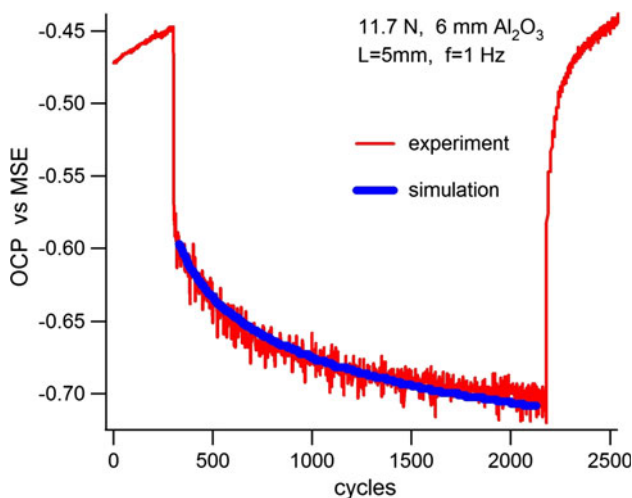


Fig. 4 Tribo-electrochemical OCP experimental curve and the mathematical simulation (superposed) for the stellite 21 sample in 0.5 M H₂SO₄ at 11.7 N normal load, showing the close agreement of the OCP evolution prediction with the experimental response

that the first stroke of the tribocorrosion experiment is considered to result in a finite starting wear volume defined by the stroke length and the cross-sectional circular segment area of the initial impingement of the pin, i.e., $V_{\text{init}} = L * A_{\text{cs,init}}$, implying that the rubbing does not commence from $A_{\text{wt}} = 0$, but rather from a calculated finite value, as seen in Fig. 3. The model determines an appropriate initial impingement diameter here of 101 μm, after which the rubbing continues with the variation of A_{wt} with cycle number being a function of time to the power of 1/3, as prescribed by Eq. (9). The OCP experimental and simulated curves are finally depicted in Fig. 4.

The high accuracy of the OCP simulation for this system indicates that possible sources of error that could result in important deviations from ideal galvanic coupling behavior as described by the general model are to a great degree absent. Systems that may, e.g., generate electrochemically active third body particles outside the wear track, or when the wear rate constants of the systems are influenced by significant work hardening or other unforeseen factors during rubbing, are susceptible to deviations from the model. Also, an unaccounted for “running-in” period in the initial phase of the experiment can limit the accuracy of the model, if it is significant in magnitude.

4.2 Ti Pure (99.6 %) in 0.14 M NaCl

For the case of pure Ti metal in 0.14 M NaCl and with model parameter $i_a = 5 \text{ mA/cm}^2$, the simulation of the experimental OCP versus time (or cycle number) curve (Fig. 5), defines the one and only C_w for each load, i.e., 0.5, 3, and 7 N, taking also into account the experimental polarization curve produced for this material (Fig. 6). The wear behavior strictly follows Archard's law from the onset of rubbing up until a given time or cycle number, different for each load experiment; from this point onward, wear is seen to deviate from the initial wear mechanism, as witnessed from the divergence from the anticipated OCP trend with time—most probably related to an Archard's wear equation breakdown. This implies that the model can only

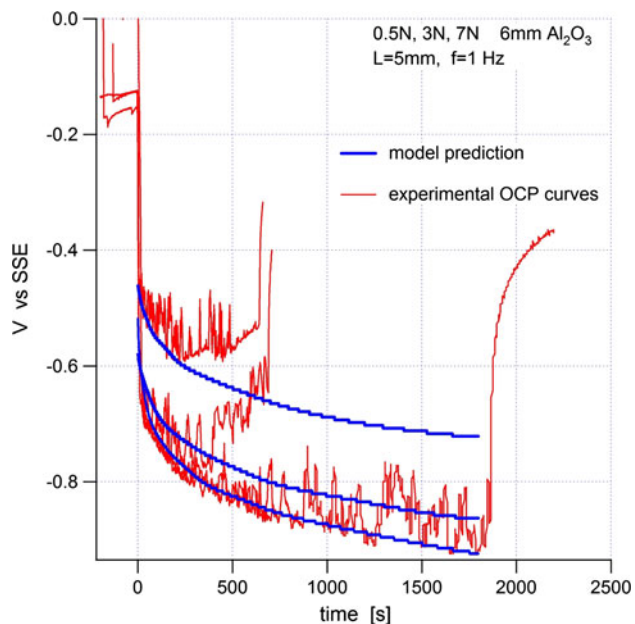


Fig. 5 Tribo-electrochemical OCP experimental curves corresponding to 0.5, 3, and 7 N normal loads along with the mathematical simulation (superposed) estimated from best fit of the model potential with the i_a as variable parameter. System is Ti (99.6 %) in 0.14 M NaCl

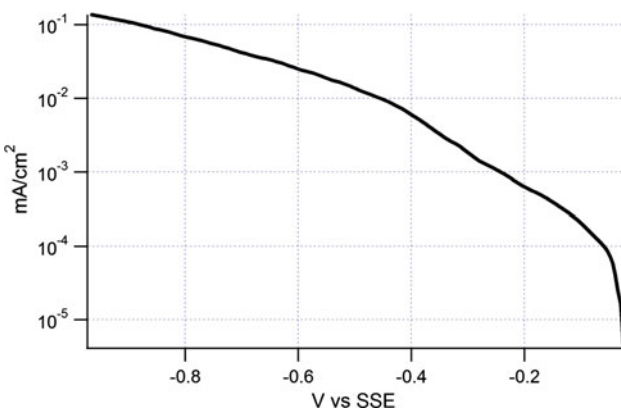


Fig. 6 The cathodic polarization curve for Ti (99.6 %) in 0.14 M NaCl, which was utilized in the tribo-electrochemical OCP model of Fig. 5

correctly predict quantities such as the wear volume V_w and the wear track surface A_{wt} from the onset of rubbing and up to a critical cycle number, different for each load as shown in Figs. 7 and 8. Furthermore, when plotting the calculated C_w corresponding to each of the three loads in the Archard's consistent time domains, the model predicts the linear relation of C_w with F_n as expressed in Archard's wear, i.e.,

$$C_w = K_w F_n 2 L f / H \quad (12)$$

where f is the frequency, H is the material hardness, and L is the scar length.

Although it is anticipated that the model provides a single C_w value for each F_n , as derived from the slope of the linear Archard's behavior $V = C_w * t$, it is not self-explanatory as to how these three C_w values should necessarily lie on a straight line intercepting the origin of a C_w versus F_n plot (see Fig. 9), as each mathematical interpolation for each experimental OCP curve is independently performed to best fit, with a common value for the model parameter $i_a = 5 \text{ mA/cm}^2$ taken in all three cases, which is an imperative reflecting the material and its repassivation kinetics in the electrolyte studied, expected to be of the same order in all cases. The above result is ultimate proof that Eq. (11) holds in all three cases and that the principle wear mechanism in the initial phase of each experiment appears to be unchanged, until it reaches the cycle when the deviation from Archard commences. This fact dictates a wear coefficient K_w , of constant value in the expression C_w versus F_n of Eq. (12), a fact that can be reasonably assumed as the variations in K_w and H are expected to be negligible for the same body–counterbody–electrolyte system.

These cycle number limits represent different rubbing times for different normal forces F_n , and the sliding experiments manifest this limitation, as the wear law after that point ceases to be described mathematically by Archard's

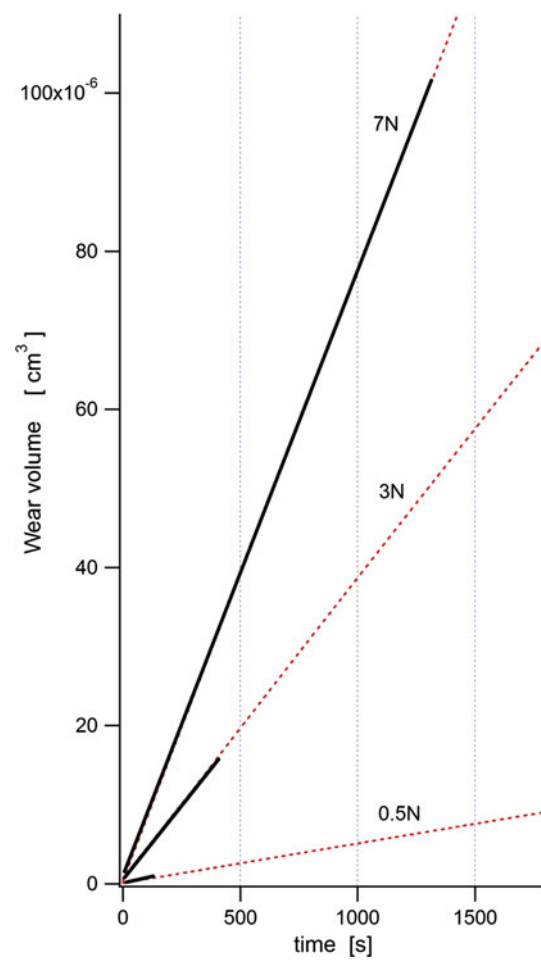


Fig. 7 The total wear volume until the experimental limit (solid lines) plotted against time, along with the model's calculated volume loss (dashed lines) as a function of time for the Ti (99.6 %) in 0.14 M NaCl system under tribocorrosion at 0.5, 3, and 7 N normal loads

equation, i.e., Eqs. (11)–(12), apparently owing to insufficient F_n normal force for the increasing surface contact conditions developing during wear (decrease in average contact pressure), thus causing a severe deviation from the initial pressure predicted by Hertzian contact mechanics. This effect has direct consequences in conjunction with plastic flow and/or the asperity deformation mechanism assumed in the Archard's wear formulation, which is a prerequisite initially satisfied by design and usually defined by the counterbody diameter and the choice of formal force, which should result in Hertzian contact pressures well above the yield strength of the tested material. Figures 7 and 8 depict the cycle limits up to which the simulation correctly reflects the experimental OCP and are different for each normal force tested: ca. 1300, 400, and 100 cycles for normal forces 7, 3, and 0.5 N, respectively.

It is noted that the model predictions of the OCP evolution with cycle number and equally for the wear volume

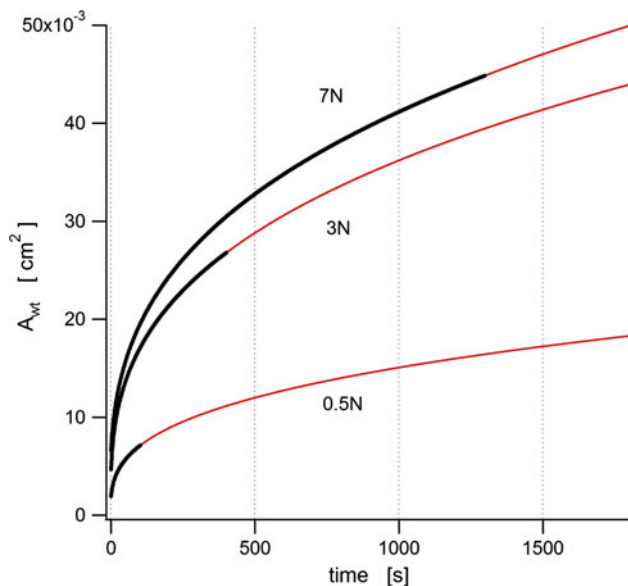


Fig. 8 The plots of wear track's surface area with time corresponding to each normal load as calculated from model for the Ti (99.6 %) in 0.14 M NaCl system under tribocorrosion at 0.5, 3, and 7 N normal loads. The **bold lines** represent the experimentally observed limits, while the continuation indicates the theoretical values under Archard's wear

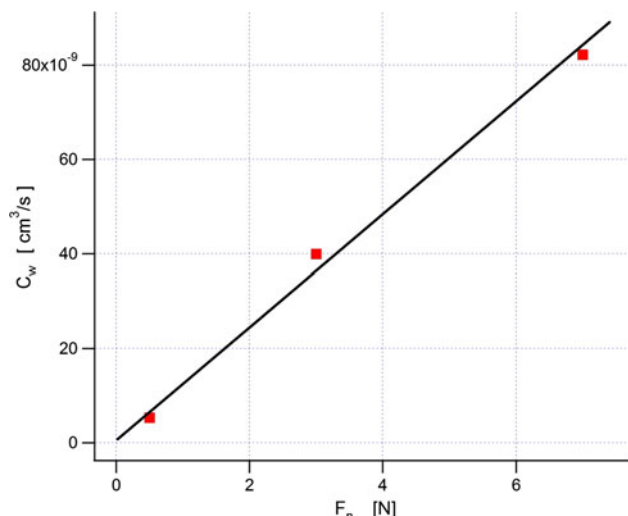


Fig. 9 The model's calculated wear constants plotted against the normal load for the Ti (99.6 %) in 0.14 M NaCl system under tribocorrosion. Note the experimental volume data (squares) are consistent with the calculated wear constants which closely exhibit linear behavior with normal load

V_w accurately reflect the experimental data. For example, at 7 N, the experimental wear volume measurements by profilometry at 40 and 450 cycles produced V_w values consistent within a SD of $\pm 7\%$ for the C_w value of $8.1 \times 10^{-9} \text{ cm}^3/\text{s}$ determined through the convergence of the model with the experimental OCP curve. (see Fig. 7).

Surprisingly, the model can also serve as a guide to indicate ideal wear behavior to which experimental trends away from the theoretically predicted can be compared and tentatively explained. From an electrochemical point of view, a trend toward leveling off and stabilization or an upward OCP trend indicates that the total depassivated surface of the wear track is either increasing at a lower rate, remaining constant, or is decreasing with cycle number, respectively. The effects demonstrated in the experimental results after the Archard's limit can therefore be better explained on the basis of a change in wear mechanism. Although the decrease of an Archard's law constant resulting in a decrease in wear rate could sufficiently explain the trend at 7 N, a dramatic change in wear mechanism after Archard's breakdown is more plausible than an unmitigated wear track surface variation, especially for 3 and 0.5 N, which is consistent with a stable third body metal/oxide tribo-layer being formed during rubbing and totally dominating the wear rate [22].

From first approximation calculations of the contact surface at the breakdown limit using the track width dimensions predicted by the model (also verified by measurement) and associating these with calculated Hertzian contact pressures derived from contact surface (ellipsoidal) semimajor a and semiminor b axes of the ball on the concave wear track for the three loads, it is revealed that (see Table 1) the $P_{av@lim}$ values are very closely situated within the range of the reported yield strength of the metal, i.e., 140–240 MPa.

From the Hamrock–Dowson approximation [23] for the contact parameter calculation of a convex on a concave body, we find that (see Appendix)

$$P_{av@lim} = \left(\frac{E' W}{6\pi\bar{\epsilon}Ra} \right)^{1/2} \quad (13)$$

where $a = 0.5 a_{@lim}$ and $a_{@lim}$ is the track width at the breakdown limit.

The above analysis indicates that $P_{av@lim}$, i.e., the P_{av} at the Archard's breakdown limit, most probably assumes a

Table 1 Contact mechanical data for Ti metal before rubbing along with the calculated properties at the breakdown limit

	7 N	3 N	0.5 N	Hertzian mechanics
P_{av}	723	545	300	
a	111	83	46.1	
Archard limit (cycle)	1300	400	100	
$a_{@lim}$	903	535	140	
$P_{av@lim}$	220 ± 31	191 ± 8	160 ± 10	

Note that P_{av} is the Hertz average contact pressure and a is the Hertzian contact diameter before sliding (ball on plane)

value ca. 190 MPa for all the three experiments with varying loads (see Table 1). Taking this approach a step further, the correlation between load and Archard's limit corroborates as evidence that the $P_{av@lim}$ value found so close to the yield strength of the material (reported yield strength 140–240 MPa) must not be incidental and leads us to deduce that, within calculation error and unaccounted for influences such as surface roughness, counterbody adhesion, and third body effects, the Archard's law requirement for surface plastic deformation must be the underlying cause of the tribocorrosion behavior beyond the cycling limits exhibited with load variation.

4.3 Al Alloys in 0.05 M NaCl

As described above, the simulation process, resulting from the best fit of an experimental OCP curve from a given material and under given specific physical/electrolyte conditions of a tribometric experiment, uniquely defines two variable parameters, i.e., i_a and C_w . Considering the experimentally determined wear volumes measured at 600 cycles for the differently heat-treated alloys studied previously [6], the problem rests only in adjusting the i_a parameter value.

In the case of the above mentioned tribocorrosion of Al alloys, which differ in their heat treatment (see Fig. 10), the experimental wear volumes measured are: $20e-6 \text{ cm}^3$ at 600 cycles for the Al-S2h sample; and $35e-6 \text{ cm}^3$ at 600 cycles for the Al-NHT sample, also shown as graphical representation in Fig. 11. The model's determined parameters for the

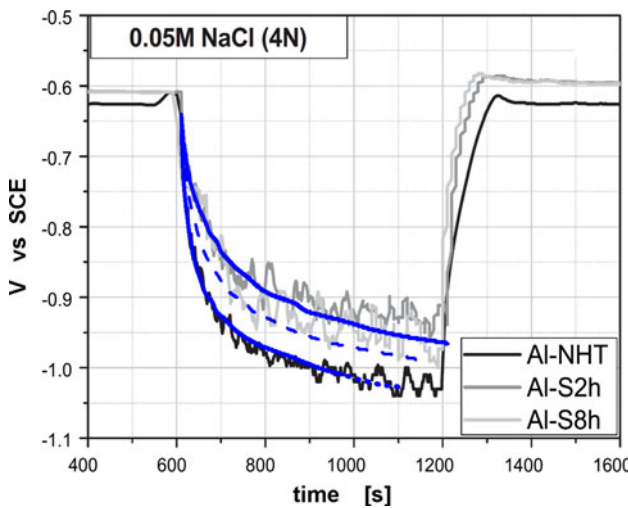


Fig. 10 Tribo-electrochemical OCP experimental curves of Al alloys in 0.05 M NaCl under 4 N normal load [6] along with the mathematical simulation (superposed) determined on the basis of experimental wear loss data for each alloy and by best fit of the model's potential with the i_a as variable parameter. The dashed line represents the simulation result for the Al-NHT experiment, but with $i_a = 11 \text{ mA/cm}^2$ (the fitted Al-S2h current) instead of 14 mA/cm^2

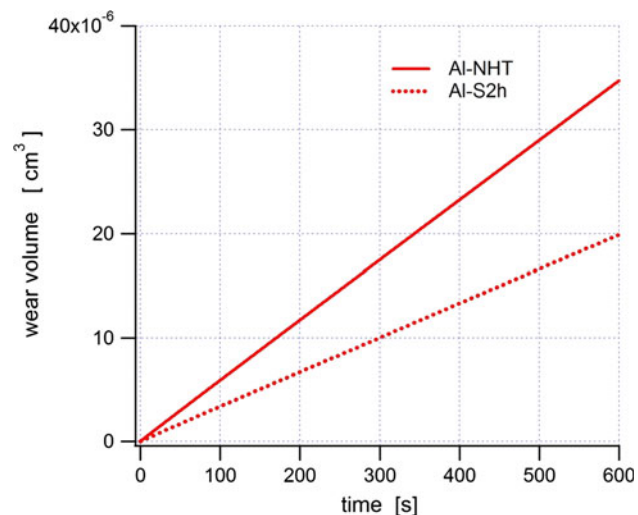


Fig. 11 The total wear volume trend with cycle number or time for the Al alloys tested, extracted from the discrete experimental data points and re-plotted as a continuous function of time, representing the sample wear in 0.05 M NaCl under tribocorrosion and 4 N normal load

best fit to each experimental OCP curve, respectively, are $i_a = 11 \text{ mA/cm}^2$ and $C_w = 3.52e-8 \text{ cm}^3/\text{s}$ for Al-S2h; and $i_a = 14 \text{ mA/cm}^2$ and $C_w = 6.15e-8 \text{ cm}^3/\text{s}$ for Al-NHT.

In summary, given the identical experimental polarization curves in the studied cathodic region [6] and the knowledge of the experimental wear volumes, it is necessary that two parameters are adjusted for a best fit to the experimental OCP data: i_a and C_w . This by itself is suggestive of a change in the depassivation/repassivation dynamics or/and in the effective surface area or the microscale surface morphology, combined with the change in the physical/mechanical properties due to the different heat treatments of the samples compared, i.e., hardness etc. However, microscopic examination of the topography of these wear scars does not present evidence of such a difference with respect to track surface morphology [6].

In order to facilitate the development of an alternative hypothesis, the above results are presented in ratio form (subscript 1 = Al-S2h and 2 = Al-NHT). Given that $V_{w1}/V_{w2} = 20/35 = 0.571$ from measurement, the best fits of the variable parameters of the model, as stated above for this case, were determined to be

$$C_{w1}/C_{w2} = 3.52e-8/6.15e-8 = 0.572 \text{ and } i_{a1}/i_{a2} = 0.78$$

In order to appreciate the consequence of the above results, it is noted that according to Archard's law, i.e., $V = C_w * t$, where $C_w = K_w F_n 2L f/H$, as well as from the known and experimentally determined hardness values taken from indentation measurements [6], we have for the

two alloy specimens prepared under different thermal conditions:

$H_2/H_1 = 0.69 \pm 0.01$ and on applying Eq. (12) for the two samples we get

$$C_{w1}/C_{w2} = H_2/H_1 * K_{w1}/K_{w2} \quad (14)$$

By substituting the numerical values for C_{w1}/C_{w2} and H_2/H_1 presented above into Eq. (14), we derive the ratio of the dimensionless wear coefficients $K_{w1}/K_{w2} = 0.83$. This value is therefore 17 % smaller than the theoretically expected value of 1, which reflects the case of similar samples under the same conditions, and no change in the wear mechanism. A subtle yet influential change in wear mechanism between these two differently treated alloys is thus implied.

The value $i_{a1}/i_{a2} = 0.78$, i.e., the 22 % increase in the i_a of the Al-NHT alloy, could be explained by a corresponding 22 % increase in the specific surface area due to the higher dispersion of the secondary constituent phases, which may have resulted in influencing the micro-morphology of the scar surface. However, this fact alone does not sufficiently justify the 17 % increase in the wear coefficient K_w calculated on the basis of a manifestly valid Archard's law and the experimental wear scar hardness measurements. On the contrary, track surface morphology/topography appears very similar in both alloys studied [6], suggesting that a difference in surface area can only make an insufficiently small contribution to the anode repassivation currents.

In conclusion, the most prominent factor should therefore be the difference in the chemical wear contribution, as expressed by the formula: $V_w = V_{\text{mech}} + V_{\text{chem}}$. Indeed, an increase in V_{chem} by 22 % for the Al-NHT material readily justifies the difference in anode currents assumed, i.e., $i_{a1}/i_{a2} = 0.78$, given the proportionality of V_{chem} and i_a , according to the relation of equivalence of oxide volume to the repassivation charge obtained through substitution from Eq. (4): $V_{\text{chem}} = i_a * (M/3\rho Ff)$, where M and ρ are the molecular weight and density of the oxide, respectively. Here, the dissolution current is considered negligibly small as i_{corr} at OCP for these alloys has been estimated from experimental polarization resistance measurements [24] to be in the range $10^{-2}\text{--}10^{-3} \text{ mA/cm}^2$, i.e., 2–3 orders of magnitude smaller than the repassivation current levels.

To explain this point further, in the case of wear-accelerated corrosion, V_{chem} can be better defined as the aggregate alloy volume loss due to the dissolution current and the repassivation current contributions. A presumed difference in any of the above current levels can finally result synergistically along with the finer microstructural properties of the Al-NHT substrate, in a passive layer with sufficiently different physical, and consequently mechanical, wear characteristics. This could consequently justify the derived difference in the dimensionless wear coefficients, i.e., $K_{w1}/K_{w2} = 0.83$, which is the indicator of a

more or less subtle change in wear mechanism. Evidence for substantiating the above effects can be found in (a) the larger contribution of the measured V_{chem} to the total wear for the Al-NHT samples reported for the tribocorrosion at, e.g., slightly higher anodic or cathodic potentials to the E_{corr} , as evidenced by the recorded higher incremental jump in the anodic currents with the onset of rubbing [6]; as well as in (b) the measurable hysteresis exhibited (i.e., lower current densities) in the heat-treated alloy polarization curves as compared with Al-NHT, over most of the passive region, which eventually undergoes transition into a passive state with the same passive current for all samples, as reported in previous publications [6, 24].

In summary, adding to the predictive capability of this model is the realization that the OCP behavior of the Al-NHT cannot be correctly recreated by the incorporation of the measured higher C_w value alone into the model calculation and assuming an unchanged i_a parameter for both samples. In order to elucidate this aspect, Fig. 10 depicts the model OCP based on the same C_w value (i.e., $6.15 \times 10^{-8} \text{ cm}^3/\text{s}$) corresponding to the experimentally determined volume loss for the Al-NHT alloy, but this time calculated on the basis of an identical anode current density to the Al-S2h, i.e., 11 mA/cm^2 . Comparison with the experimental OCP curve shows that the adjustment of the C_w as model variable is apparently insufficient to reproduce the real OCP trend. For the Al-NHT alloy, only the combined increase of the C_w and i_a can finally lead to the faithful reproduction of the experimentally observed OCP behavior. From a theoretical point of view, the higher repassivation current assumed for the non-heat-treated Al-NHT alloy is in broader agreement with the well-established concepts of easier ion movement along grain boundaries and imperfections [25], which also extends into the growth of the oxide passive layers [26], as a higher degree of grain boundary defects exists in the case of the non-aged/non-recrystallized Al-NHT sample, as compared with the heat-treated sample Al-S2h [24].

5 Conclusions

This study has provided new valuable insights into the wear-corrosion behavior of the metals, as well as into the tribocorrosion field. The development of successful simulation models for tribocorrosion experiments have already contributed to the rationalization of such controlled wear-accelerated experiments and their OCP behavior under rubbing. These results concretely demonstrate that even rudimentary mathematical models of controlled tribo-electrochemical contacts can complement the physical experiment and add valuable understanding to the tribological behavior of metals, alloys, and generally to materials in an electrochemically active environment.

The stellite material test has demonstrated that the galvanic coupling model is, beyond doubt, extremely accurate in predicting OCP evolution with time as well as the wear rate or wear volume loss with cycle number, when conditions for Archard wear are fulfilled. The excellent agreement of all experimental wear data and the experimental OCP curve with the model-generated volume loss/wear rate parameters and the OCP simulation with time establishes the concepts underlying the galvanic coupling model as a valid methodological approach toward a quantitative description and mechanistic understanding of the tribo-electrochemical experiment. The implications of secondary parameter generation from the model, such as average wear track current density, i_a , have not as yet been fully explored. The prediction of an average wear track (anode) potential E_a is clearly also possible, when electrolyte properties, cell geometry, and current distribution can be calculated, thus allowing for the estimation of the resistance between anode and cathode.

In the example of Al alloys, the model has helped us discern and better quantify the relative contributions of chemical and mechanical wears and, in particular, revealed the underlying synergy in the total wear mechanism, otherwise undetectable in single experiments because of the convoluted nature of the experimental responses.

The example of Ti metal tribocorrosion under variable load has assisted in demystifying the so-often observed change in the trend of the OCP curve with advancing cycle number. The model has revealed that the contact pressure P_{av} , mostly assumed well above the plastic limit to assume Archard's wear behavior throughout an experiment, can reach much lower values within the experimental time domain and finally be the cause of interruption of the initial wear mechanism. After hitting a critical lower limit $P_{av@lim}$ at a given cycle, the subsequent cycles proceed with unchanged or a variable wear rate that is decidedly lower than the initial value, thereby resulting in the OCP stabilization and the eventual reversal of the normal trend toward more negative potentials with increasing cycle number. This system can serve as a general paradigm that may help us elucidate very puzzling OCP trend changes often encountered throughout tribo-electrochemistry.

Acknowledgments The authors wish to thank S. Guadalupe for sharing experimental data on the stellite 21 material, and N. Espalargas and the IPM-NTNU for providing materials and support in making this research possible.

Appendix

Hertz Pressure

Hertz's theory is used to calculate the average pressure and maximum pressure between two non-conforming contacts.

This theory was used to assess changes in maximum pressure during wear. For this purpose, the equations established by Hamrock and Dowson [23] were assumed. Therefore, the dimensions of contact (assumed elliptical) are given by Eq. I, where a is the semimajor axis and b the semiminor axis of the contact.

$$a = \left(\frac{6\bar{k}^2\bar{\varepsilon}WR'}{\pi E'} \right)^{1/3} \quad (I)$$

$$b = \left(\frac{6\bar{\varepsilon}WR'}{\pi\bar{k}E'} \right)^{1/3}$$

where $\bar{\varepsilon}$ is a simplified integration parameter and \bar{k} a parameter of ellipticity given by

$$\bar{\varepsilon} = 1.0003 + 0.5968 \frac{R_x}{R_y} \quad (II)$$

$$\bar{k} = 1.0339 \left(\frac{R_y}{R_x} \right)^{0.636}$$

where E' is the reduced Young's modulus, R' is the radius of reduced curvature, and R_x and R_y are the reduced radii in the x -direction and the y -direction, respectively. The x and y axes are defined as the axes of the plane of the contact, respectively, along the major axis and minor axis of the ellipse formed by it. These values are defined as

$$\frac{1}{E'} = \frac{1}{2} \left(\frac{1 - v_a^2}{E_a} + \frac{1 - v_b^2}{E_b} \right)$$

$$\frac{1}{R_x} = \frac{1}{R_{bx}} + \frac{1}{R_{ax}}$$

$$\frac{1}{R_y} = \frac{1}{R_{by}} + \frac{1}{R_{ay}}$$

$$\frac{1}{R'} = \frac{1}{R_y} + \frac{1}{R_x}$$

where E_a and E_b are the Young's modulus values of the material of body a and body b; v_a and v_b their respective Poisson coefficients; R_{ax} , R_{bx} , R_{ay} , and R_{by} are the radii of curvatures of the body a along the x axis, the body b along the x axis, and body a along the y axis, and body b along this same axis, respectively.

In the case studied, it was assumed that the contact is between the sphere (i.e., the ball) and the concave track surface having a radius of curvature R_{by} , which is considered here only slightly larger than the curvature of the ball of radius $R = R_{ax} = R_{ay}$.

According to Eq. I and II of the above method, the average contact pressure exerted by the sphere onto the concave track, under force W , is given by

$$P_{av} = W/\pi ab \quad (III)$$

Using the definitions declared in the Sect. 4 and substituting Eq. I, II into Eq. III we have

$$P_{av@lim} = \left(\frac{E' W}{6\pi\bar{\varepsilon}Ra} \right)^{1/2}$$

where $a = 0.5 a_{@lim}$ and $a_{@lim}$ is the wear track's width.

References

- Landolt, D., Mischler, S., Stemp, M.: Electrochemical methods in tribocorrosion: a critical appraisal. *Electrochim. Acta* **46**, 3913–3929 (2001)
- Jemmely, P., Mischler, S., Landolt, D.: Electrochemical modeling of passivation phenomena in tribocorrosion. *Wear* **237**, 63–76 (2000)
- Olsson, C.-O.A., Landolt, D.: Passive films on stainless steels—chemistry, structure and growth. *Electrochim. Acta* **48**, 1093–1104 (2003)
- Burstein, G.T., Liu, C.: Time-resolved electrochemical impedance of the guillotined aluminium electrode. *Electrochim. Acta* **39**, 873–882 (1994)
- Burstein, G.T., Organ, R.M.: Repassivation and pitting of freshly generated aluminium surfaces in acidic nitrate solution. *Corros. Sci.* **47**, 2932–2955 (2005)
- Vieira, A.C., Rocha, L.A., Papageorgiou, N., Mischler, S.: Mechanical and electrochemical deterioration mechanisms in the tribocorrosion of Al alloys in NaCl and in NaNO₃ solutions. *Corros. Sci.* **54**, 26–35 (2012)
- Julian, L.C., Munoz, A.I.: Influence of microstructure of HC CoCrMo biomedical alloys on the corrosion and wear behaviour in simulated body fluids. *Tribol. Int.* **44**, 318–329 (2011)
- Cawley, J., Metcalf, J.E.P., Jones, A.H., Band, T.J., Skupien, D.S.: A tribological study of cobalt chromium molybdenum alloys used in metal-on-metal resurfacing hip arthroplasty. *Wear* **255**, 999–1006 (2003)
- Munoz, A.I., Julian, L.C.: Influence of electrochemical potential on the tribocorrosion behaviour of high carbon CoCrMo biomedical alloy in simulated body fluids by electrochemical impedance spectroscopy. *Electrochim. Acta* **55**(19), 5428–5439 (2010)
- Benea, L., Ponthiaux, P., Wenger, F., Galland, J., Hertz, D., Malo, J.Y.: Tribocorrosion of stellite 6 in sulphuric acid medium: electrochemical behaviour and wear. *Wear* **256**(9–10), 948–953 (2004)
- Stack, M.M., Huang, W., Wang, G., Hodge, C.: Some views on the construction of bio-tribo-corrosion maps for titanium alloys in Hank's solution: particle concentration and applied loads effects. *Tribol. Int.* **44**, 1827–1837 (2011)
- Galliano, F., Galvanetto, E., Mischler, S., Landolt, D.: Tribocorrosion behavior of plasma nitrided Ti6Al4 V alloy in neutral NaCl solution. *Surf. Coat. Technol.* **145**, 121–131 (2001)
- Mischler, S.: Triboelectrochemical techniques and interpretation methods in tribocorrosion: a comparative evaluation. *Tribol. Int.* **41**, 573–583 (2008)
- Barril, S., Mischler, S., Landolt, D.: Influence of fretting regimes on the tribocorrosion behaviour of Ti6Al4 V in 0.9 wt% sodium chloride solution. *Wear* **256**, 963–972 (2004)
- Mindivan, H., Baydogan, M., Kayali, E.S., Cimenoglu, H.: Wear behaviour of 7039 aluminum alloy. *Mater. Charact.* **54**, 263 (2005)
- Bouaeshi, W.B., Li, D.Y.: Effects of Y₂O₃ addition on microstructure, mechanical properties, electrochemical behavior and resistance to corrosive wear of aluminum. *Tribol. Int.* **40**, 188–199 (2007)
- Li, J., Elmadaagli, M., Gertsman, V.Y., Lo, J., Alpas, A.T.: FIB and TEM characterization of subsurfaces of an Al–Si alloy (A390) subjected to sliding wear. *Mater. Sci. Eng. A* **421**, 317–327 (2006)
- Landolt, D.: Corrosion and Surfaces Chemistry of Metals, 1st (edn). EPFL Press, Lausanne (2007)
- Krawiec, H., Vignal, V., Heintz, O., Ponthiaux, P., Wenger, F.: Local electrochemical studies and surface analysis on worn surfaces. *J Electrochem Soc* **155**(3), C127–C130 (2008)
- Landolt, D., Mischler, S., Stemp, M.: Electrochemical methods in tribocorrosion: a critical appraisal. *Electrochim. Acta* **46**(24–25), 3913–3929 (2001)
- Stojadinovic, J., Bouvet, D., Declercq, M., Mischler, S.: Effect of electrode potential on the tribocorrosion of tungsten. *Tribol. Int.* **42**, 575–583 (2009)
- Barril, S., Mischler, S., Landolt, D.: Electrochemical effects on the fretting corrosion behavior of Ti6Al4 V in 0.9 % sodium chloride solution. *Wear* **259**, 282–291 (2005)
- Hamrock, B.J., Dowson, D.: Ball Bearing Lubrication—The Elastohydrodynamics of Elliptical Contacts. Wiley, New York (1981)
- Vieira, A.C., Pinto, A.M., Rocha, L.A., Mischler, S.: Effect of Al₂Cu precipitates size and mass transport on the polarisation behavior of age-hardened Al–Si–Cu–Mg alloys in 0.05 M NaCl. *Electrochim. Acta* **56**, 3821–3828 (2011)
- Kröger, F.A.: The Chemistry of Imperfect Crystals, 2nd edn. Elsevier, New York (1973)
- Boxley, C.J., White, H.S., Gardner, C.E., Macpherson, J.V.: Nanoscale imaging of the electronic conductivity of the native oxide film on titanium using conducting atomic force microscopy. *J. Phys. Chem. B* **107**, 9677–9680 (2003)